

Airway remodelling with spatial correlations: Implications for asthma pathogenesis



Christopher D. Pascoe^a, Francis H.Y. Green^b, John G. Elliot^c, Alan L. James^d, Peter B. Noble^e,
Graham M. Donovan^{f,*}

^a Children's Hospital Research Institute of Manitoba, Department of Physiology and Pathophysiology, University of Manitoba, Winnipeg, Manitoba, Canada

^b Department of Pathology and Laboratory Medicine, Cumming School of Medicine, University of Calgary, Calgary, Alberta, Canada

^c West Australian Sleep Disorders Research Institute, Department of Pulmonary Physiology and Sleep Medicine, Sir Charles Gairdner Hospital, Nedlands, Western Australia, Australia

^d Department of Pulmonary Physiology and Sleep Medicine, Sir Charles Gairdner Hospital, School of Medicine and Pharmacology, The University of Western Australia, Australia

^e School of Human Sciences, The University of Western Australia, Crawley, Western Australia, Australia

^f Department of Mathematics, University of Auckland, Private Bag 92019, Auckland Mail Centre, Auckland 1142, New Zealand

ARTICLE INFO

Keywords:

Airway smooth muscle
Mechanotransduction
Bronchoconstriction

ABSTRACT

Airway remodelling is a cardinal feature of asthma in which airways undergo structural changes - in particular, increased airway smooth muscle mass and total airway wall area. Remodelling has long been thought to have functional consequences in asthma due to geometric effects that can increase airway narrowing and luminal occlusion. Prior studies have examined the distribution of remodelling between and within patients, but none have yet considered the possibility for *spatial correlations* in airway remodelling. That is, is remodelling clustered locally, or interrelated along proximal and distal locations of the bronchial tree? In view of recent interest regarding airway remodelling produced by mechanical stimuli, we developed a mathematical model to examine whether spatial correlations in airway remodelling could arise due to cycles of bronchoconstriction and mechanotransduction. Further, we compared modelling predictions to the spatial distribution of airway remodelling in lungs from subjects with and without asthma. Results indicate that spatial correlations in airway remodelling do exist *in vivo*, and cycles of bronchoconstriction and mechanotransduction are one plausible mechanism for their origin. These findings offer insights into the evolution of airway remodelling in asthma, which may inform strategies for treatment and prevention.

1. Introduction

'Airway remodelling' is an important feature of asthma, in which airways undergo structural modification, particularly increased thickness of the airway smooth muscle (ASM) layer and total wall thickness (Redington and Howarth, 1997; Stewart, 1996). While it has long been understood that the extent of airway remodelling contributes to airflow limitation (Bai et al., 1998; James and Wenzel, 2007), what has yet to be established is how remodelling across different airways is organized relative to one another - i.e. the *spatial* distribution of remodelling is unclear. Are airways with greater remodelling likely to occur near one another (on a local or regional basis), and/or are remodelling processes organized along interconnected branching pathways, or across disconnected airways in close proximity? Distribution of airway remodelling has been shown to be an important determinant of the final

organ response, such as total lung resistance and compliance; for example, increased heterogeneity of airway remodelling produces greater functional impairment compared with a more homogenous distribution (Thorpe and Bates, 1997; Gillis and Lutchen, 1999; Pascoe et al., 2017b)

A separate but interrelated question relates to how such correlations in airway structure develop, which is directly relevant to the origin of airway remodelling in disease. One of the most influential studies of airway remodelling in recent years by Grainge et al. (Grainge et al., 2011) demonstrated that bronchoconstriction alone is sufficient to produce altered airway structure. Bronchoconstriction-induced remodelling could theoretically impact at all stages of life: that is, during development where the ASM contracts *in utero* (Parvez et al., 2006), or during an acute exacerbation experienced by a child or adult who has asthma. Importantly, if bronchoconstriction via mechanotransduction

* Corresponding author.

E-mail address: g.donovan@auckland.ac.nz (G.M. Donovan).

<https://doi.org/10.1016/j.resp.2020.103469>

Received 4 February 2020; Received in revised form 30 April 2020; Accepted 21 May 2020

Available online 28 May 2020

1569-9048/ © 2020 Elsevier B.V. All rights reserved.

(Tschumperlin and Drazen, 2006; Fabry and Fredberg, 2007; Hill et al., 2018; Kılıç et al., 2020) produces remodelling, it is reasonable to assume that this may manifest as structure which is spatially correlated.

Through use of a conceptual model (Tschumperlin and Drazen, 2006; Lutchen, 2016; Lutchen et al., 2017), we tested the feasibility of the hypothesis that *spatially correlated airway remodelling could be formed by cycles of bronchoconstriction, mechanotransduction, and remodelling*; referred to here as the bronchoconstriction-mechanotransduction-remodelling (BMR) cycle. We used a previously developed multi-branch airway tree lung model, adapted to include a simple heuristic remodelling algorithm based solely on the degree of bronchoconstriction occurring in each airway throughout the tree. We then characterized the resulting remodelling distribution using measures of spatial heterogeneity, and compared these predictions with measurements of remodelling in post-mortem lungs from different patient groups.

2. Methods

This study used a combination of theoretical modelling and empirical data on airway wall thickness acquired from subjects with and without asthma. Two different methods of sampling airways from human lungs were followed: planar lung sections assessed correlations in remodelling on short length scales which are not arranged along the airway tree, while similar data sampled along branching pathways assessed correlations between interconnected airways across a broad range of generations (Fig. 1).

2.1. Model overview

The conceptual model is based on the idea that airways undergo cycles of bronchoconstriction, mechanotransduction, and remodelling (BMR cycles). This is made explicit in a mathematical model making use of an existing model of bronchoconstriction combined with a new heuristic model of mechanotransduction and remodelling. A brief conceptual outline is given here, and further details are presented in the following section. We make use of an existing functional model to

determine the bronchoconstriction patterns which occur in each cycle (Donovan, 2017; Donovan et al., 2018). This model uses the detailed structure of the airway tree, including airway connectivity, dimensions, and structural properties such as basement membrane perimeter (P_{bm}), ASM area, and total wall area (WA) for each airway to compute lung function both in terms of overall flow patterns and respiratory resistance. Importantly this is done in the presence of induced ASM tone and hence bronchoconstriction. The fundamental elements are the airway model of (Lambert et al., 1982), the parenchymal tethering model of (Lai-Fook, 1977), and the airway interdependence ideas of (Anafi and Wilson, 2001). The model shares some common features with the well-known symmetric tree model of (Venegas et al., 2005), but is here extended to apply to anatomically accurate structures and scaled to a whole human lung (Donovan, 2017; Donovan et al., 2018). For more details, the reader is referred to both the following section and earlier studies (Donovan and Kritter, 2015; Donovan, 2017).

For each cycle, remodelling (via mechanotransduction) is determined based on the calculated bronchoconstriction, which is assumed to occur throughout ventilation defects and low ventilation areas (Tgavalekos et al., 2005). Hence the mechanotransduction and remodelling processes also occur throughout these regions. In the absence of specific data, we make the simplest assumption and assume that remodelling, via mechanotransduction, is linearly proportional to the degree of bronchoconstriction. We also perform an extensive sensitivity analysis. For reasons of computational cost, in whole-lung simulations we use a relatively large degree of remodelling per cycle, and hence a relatively small number of cycles; as per the sensitivity analysis, the results are qualitatively unchanged from those assuming a smaller degree of remodelling per cycle, but a larger number of cycles. The important aspect, then, is not the absolute number of cycles, but rather the progression with additional cycles.

2.2. Details of mathematical model

The mathematical model of BMR cycles used in this study is a combination of an existing model of bronchoconstriction, and a new

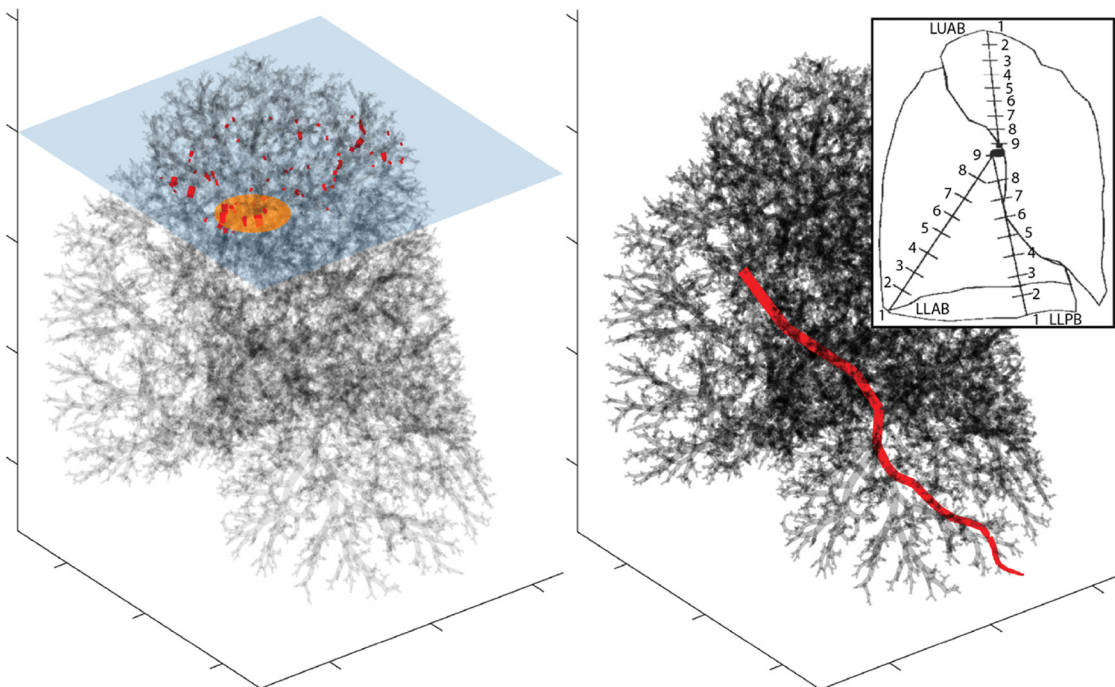


Fig. 1. Schematic illustration of sampling methods. Left panel: transverse planar sampling, with transverse plane (blue) and core (orange), and in-slide airways marked in red. Note that the core is enlarged for visibility and not shown to scale. Right panel: pathway sampling. In both cases the figure is illustrative of the method rather than indicating specific locations, e.g. for transverse planar sampling, slides are taken from multiple locations, and not just the upper lobe. Similarly, pathway sampling occurs along axial paths in each lobe (see inset).

Table 1
Patient demographics for transverse planar sampling. Pbm = Perimeter of the basement membrane.

	Non-asthma (n = 9)	Asthma (n = 12)
Median Age	20 (4–63)	15 (8–36)
Male Sex - # (%)	4 (55.6)	5 (41.7)
Inhaled Corticosteroids - # (%)	0 (0)	8 (66.7)
Smoking - # (%)	2 (22.2)	4 (33.3)
End of life steroids - # (%)	3 (33.3)	9 (75.0)
Fatal Asthma - # (%)	N/A	8 (66.7)
Pbm, mm - Mean \pm SD	3.1 \pm 0.25 mm	3.5 \pm 0.27 mm

heuristic model of the mechanotransduction and remodelling portions. Each model is applied sequentially to simulate the evolution of structure and function over repeated BMR cycles.

The bronchoconstriction model uses details of airway tree structure (branching pattern, airway lengths, airway wall parameters including basement membrane perimeter, wall area and ASM area) to predict function and flow patterns during bronchoconstriction (Donovan, 2017; Donovan et al., 2018). The fundamental elements are the airway model of (Lambert et al., 1982), the parenchymal tethering model of (Lai-Fook, 1977), and the airway interdependence ideas of Anafi and Wilson (Lai-Fook, 1977; Anafi and Wilson, 2001). With the airway and lung structure determined, we calculate the resulting flow patterns. We use the model of (Donovan, 2017), which is based on the Anafi-Wilson instability (Anafi and Wilson, 2001; Venegas et al., 2005; Leary et al., 2014). The interested reader is referred to these references for full details, but briefly the model assumes quasi-steady Poiseuille flow in each airway and describes both airway narrowing due to ASM activation, and the interactions between airways, all joined together as a very large system of coupled ordinary differential equations. Poiseuille flow and pressure balance introduce algebraic constraints, but these can be systematically eliminated (Donovan, 2016). Driving pleural pressures are determined as necessary to maintain target tidal volumes (Donovan and Kritter, 2015). The parameters of this system of equations are determined by the previous remodelling cycles, and the equations are then solved numerically in order to determine the flow patterns within that simulated lung, for a given level of ASM activation.

For the mechanotransduction and remodelling portion, we apply the following heuristic model. Mechanotransduction and remodelling are assumed to occur throughout ventilation defects as follows. Each airway, during each cycle, undergoes scaling of both WA and ASM by a factor of Δ . This is determined, for each airway and cycle, by the dynamics of the simulated agonist challenge (calculated using the model described above). We use a simple piecewise linear function

$$\Delta(\delta) = \begin{cases} 1, & \text{for } \delta \geq 1 \\ 1 + \bar{\delta}(1 - \delta), & \text{for } \delta < 1 \end{cases}$$

based on the assumption that airways which do not undergo bronchoconstriction do not undergo remodelling, and that for those that do, the remodelling is linearly proportional to the severity of the bronchoconstriction. The concept is based upon (Grainge et al., 2011), though no information is available on the precise dynamics of this process, and as such we assume the simplest plausible form. Here $\bar{\delta}$ is the parameter which determines the extent of the remodelling during each cycle, while δ is determined by the bronchoconstriction for that airway, during the challenge, and calculated for each airway as the ratio of the flow through that airway during bronchoconstriction relative to the same flow in the absence of bronchoconstriction. All airways within the simulated left lung are subject to the same remodelling process. Pbm is assumed to remain unchanged. Each simulated lung begins with a fixed branching structure, derived from CT where possible and generated algorithmically for smaller airways (Howatson Tawhai et al., 2000). All airways begin in a fictitious state with homogeneous and relatively little ASM and WA, in order to

demonstrate the spatial patterns of remodelling which emerge. A single airway tree geometry is used, based on a healthy subject. Each simulated cycle consists of average tidal breathing over 10 breaths, subject to bronchoconstriction (equal degrees of ASM activation applied everywhere). The precise timescale of a BMR cycle, however, is not explicitly specified; only the degree of remodelling which occurs in response to bronchoconstriction during the cycle.

Model simulations are performed either in a whole left lung (approximately 30,000 conducting airways), or within a restricted subtree consisting of 2133 airways. Using the whole lung is desirable where practicable, however due to the computational cost of simulation the latter is used in applications where much larger numbers of simulations are required, for example in sensitivity analysis. Parameters for the underlying functional model are as given in (Donovan, 2017). Parameter values for the additional BMR components used in the simulations were $\bar{\delta} = 0.5$ (dimensionless), and the additive noise at each cycle was zero mean and 1% standard deviation. For purposes of sensitivity analysis, $\bar{\delta}$ was tested over an order of magnitude, the noise standard deviation over $\pm 20\%$, as well as the ASM activation level over $\pm 10\%$ and the airway-airway coupling strength (see (Donovan and Kritter, 2015)) over $\pm 20\%$.

2.3. Human airway sampling – transverse planar

We collected data from post-mortem lung specimens to validate the findings from the mathematical model of BMR cycles. Subject demographics for post-mortem formalin fixed lung sections used for transverse planar sampling can be seen in Table 1. Lungs from subjects with a history of asthma were obtained with written, informed consent through the International Institute for the Advancement of Medicine (IIAM, Edison, NJ) and with approval from the University of British Columbia and St. Paul's Hospital ethics committee. Tissues from these lungs have been used in previous studies (Chin et al., 2012; Syyyong et al., 2015; Pascoe et al., 2017b, 2017a). All conditions of the ethics approvals were followed. These subjects were used for transverse planar sampling only.

Lungs were prepared for sectioning as previously described (Pascoe et al., 2017b). The method of fixation approximates an inflation pressure of 20 cm H₂O. Nevertheless, lung inflation is not a critical factor in measuring airway wall compartment areas; basement membrane perimeter (Pbm), the marker for airway size, is relatively insensitive to the degree of inflation (James et al., 1988, 2008) and the relationship between Pbm and wall areas remains largely unaffected. Transverse lung sections (5 μ m thick) were cut and then, using a sharpened hollow cylinder, cores approximately 15 mm–20 mm in diameter were sampled; the sampling procedure is illustrated schematically in Fig. 1 (left panel). An average of 5 cores per lung were used, with cores randomly sampled throughout the lung. Cores with multiple in-slide airways were used as this allowed pairwise distance measurements to be performed, with an average of 2.5 cross-sectional airways per core (n = 129 airways, n = 61 in-slide airway pairs).

2.4. Human airway sampling – pathway

Subject demographics for formalin fixed lung sections used for pathway sampling can be seen in Table 2. Whole left lungs used for pathway sampling were acquired from the Prairie Provinces Fatal Asthma Study (Tough et al., 1996; Salkie et al., 1998; Hessel et al., 1999; Boser et al., 2005; Green et al., 2010). Ethical approval for the study was obtained from the four major universities in each Canadian province involved in the study: the University of Calgary, University of Edmonton, University of Saskatchewan and the University of Manitoba. Subjects were classified as: Control (n = 31) - no history of asthma, wheeze or other lung disease; non-fatal asthma (n = 32) - death attributed to a non-respiratory cause with a confirmed history of asthma; and fatal asthma (n = 25) - death attributed to asthma with a

Table 2
Subject characteristics for pathway sampling.

	Control (n = 31)	Nonfatal asthma (n = 32)	Fatal asthma (n = 25)
Age, years, Mean \pm SD.	39 \pm 10	35 \pm 11	33 \pm 14
Gender, male / female	19 / 12	16 / 16	15 / 10
^{§§} Corticosteroid use, %: Inhaled/Oral, number (%)	–	9 (53)	12 [#] (92)
^{§§} Ever smoked, number (%)	8 (57)	11 (52)	9 (64)
Perimeter of the basement membrane, mm Mean \pm SD. (range)	12.2 \pm 1.8 (1.9–31.8)	11.3 \pm 1.6 (1.7–30.8)	11.8 \pm 1.6 (1.8–32.5)
^{§§} Body mass index Mean \pm SD. (range)	27 \pm 5* (22–38)	32 \pm 8 (16–45)	26 \pm 6* (15–41)
^{§§} Age at onset of asthma, years median (IQR)	–	17 (10–26)	9 (3–39)
^{§§} Duration of asthma, years median (IQR)	–	17 (9–21)	17 (7–22)
^{§§} Asthma severity, “Severe” number (%)	–	8 (38)	9 (64)

^{§§} = incomplete data set.

* = $p < 0.05$ v Nonfatal asthma.

= $p = 0.04$.

confirmed history. Informed consent was obtained from all families of the deceased to use the pathology samples from the autopsy for research purposes, and all conditions of the ethics approvals were followed. These lungs were used for pathway sampling only.

The main bronchus and pulmonary artery were perfused simultaneously with glutaraldehyde (2.5 % in 0.05 M phosphate buffer, pH 7.4, 350 mOsM with sucrose) at pressure heads of 20 and 40 cmH₂O respectively, thus maintaining a capillary-alveolar pressure difference of 15–20 cmH₂O. Vascular perfusion was maintained for 2 h and bronchial perfusion overnight. Three segmental bronchi, two from the lower lobe (anterior and posterior basal) and one from the upper lobe (apical), were sampled. Portions of airway (with surrounding parenchyma) were acquired at nine equidistant anatomical levels from proximal to distal locations; the sampling procedure is illustrated schematically in Fig. 1 (right panel, inset). To maintain equidistant sampling along a segment, the segment was first measured from the origin of the intrapulmonary bronchus by the most direct path to the pleural surface for that segment. Nine equally spaced blocks of tissue were obtained using cuts in the pleural surface as markers, and a 1 mm silver probe in the attendant pulmonary artery was used to identify the correct segment and to ensure that the samples were taken horizontal to the axial path. This yielded 27 airways per subject. Samples were processed into wax blocks and sectioned (5 μ m) and sections stained with hematoxylin and eosin (H & E) and an elastic trichrome technique. In total, $n = 2339$ airways were used in the analysis yielding $n = 9253$ airway pairs sampled from the same lobe (3252 NA, 3361 NFA, 2640 FA).

2.5. Morphometry

Airways were assessed by point counting. Specifically, for transverse planar sampling, tissue sections were stained with hematoxylin and eosin and airways that were determined to be near cross sectional (short to long axis ratio greater than 0.6) were included in the analysis. In-slide airway distance was calculated by measuring the minimum distance between two cross-sectional areas (center to center) on the same section for which morphometric data had been collected. More details on morphometric analysis is provided in the appendix.

Morphometry of airways acquired by pathway sampling was conducted on sections stained with the elastic trichrome technique. The areas of the ASM layer and total WA were measured by point counting. On a contiguous section stained with hematoxylin and eosin, eosinophils and neutrophils were counted within the inner airway wall around the entire airway section, based on their morphology and staining characteristics. The cell densities were calculated by normalization to total wall area. Further detail is provided in the appendix.

2.6. Spatial correlation analysis: the variogram

We used a form of analysis for spatial correlations which is well-known in geostatistics; the ‘variogram’. The variogram is more

informative than well-known measures of heterogeneity, such as the standard deviation or coefficient of variation, which are insufficient measures of spatially correlated remodelling (because they only capture information about the variation, independent of its spatial arrangement).

The variogram (Cressie and Hawkins, 1980) characterises the spatial dependence of a random field or process, and it does so as a function of the distance between two samples. Thus, the variogram is not a single value (c.f. coefficient of variation), but rather a function of the separation distance. It is calculated as:

$$\gamma(h \pm \delta) = \frac{1}{2 |N(h \pm \delta)|} \sum_{(i,j) \in N(h \pm \delta)} |z_i - z_j|^2$$

where h is the separation distance between observations (either in linear distance, or branching distance), δ is the bin tolerance, $N(h \pm \delta)$ is the set of points within that bin, and $N(h \pm \delta)$ is the number of points in that set. Here the notation z_i and z_j indicates observations from the field. Thus the variogram essentially is calculated as the sum of the squares of the differences at each separation distance, appropriately normalized. Relatively large values of the variogram indicate weaker correlations between samples separated by that distance, and conversely small values of the variogram indicate stronger correlation. The shape of the variogram therein reflects spatial dependence.

A simple illustration of the variogram as a means of quantifying spatial correlation is provided in Fig. 2. The left panel shows a random field which is spatially uncorrelated, while the center panel shows a field with significant spatial correlation/clustering. The values of both are described by the colorbar. The corresponding variograms for each are shown in the right panel. In short, in the absence of spatial correlations, the variogram is approximately constant; otherwise, the shape of the variogram characterizes the spatial correlations. Several observations are worth making: 1) this example is 2D for ease of visualization, but is essentially unchanged in 3D because it is based on the distance and variation between pairs of observations; 2) while the variogram of the data in the left panel is approximately 1, this is not exact, and does vary slightly across separation distances; and 3) the calculated variograms do not extend to zero separation distance but stop at the grid size.

We calculate two variograms in this study: a variogram based on the simple linear distance between airways, and a variogram in which the distance between airways is the tree branching distance (e.g. traced along the pathway of conducting airways connecting any two airways). Note, that because of the sampling techniques, the linear distance variogram can only be computed using the transverse planar sampling data and the branching distance variogram only from the pathway sampling data. In model simulations, both can be computed.

Variograms are computed for both total WA and ASM as measures of remodelling. In each case these areas are normalized for airway size (and non-dimensionalized) by dividing by the square of basement

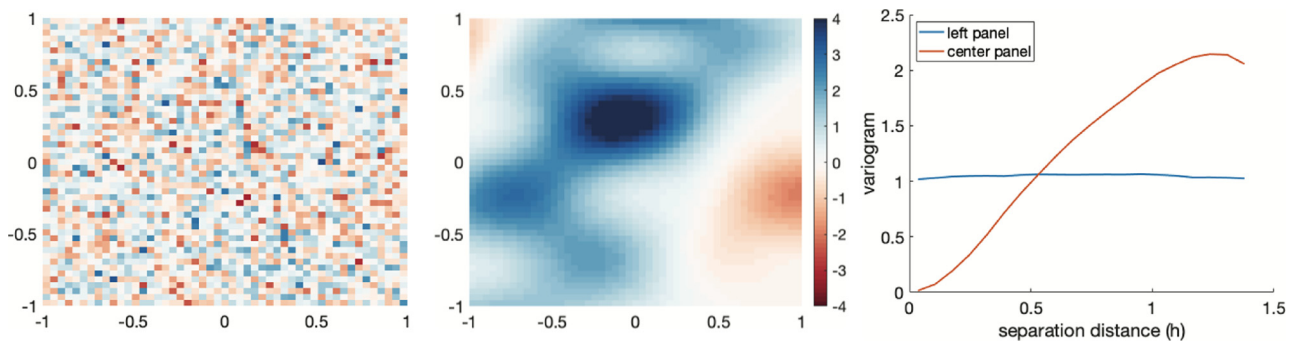


Fig. 2. Illustration of the variogram as a method of characterizing spatial correlations. Left panel: uncorrelated; center panel: correlated; right panel: corresponding variograms. See text for additional details.

perimeter (P_{bm}). Variograms are typically valid only up to a separation distance of approximately half of the maximum separation distance (known as the *distance of reliability* (Omre, 1984)), and variograms presented adhere to this convention.

For comparison with previous work, we also characterize spatial heterogeneity using a *spatial heterogeneity index* (SHI) as introduced for this purpose in (Donovan et al., 2018). This is designed to capture information about not just the overall heterogeneity, but also its spatial structure. As such it is constructed to consist of the equally weighted sum of the coefficient of variation, expressing total heterogeneity, and the spatial autocorrelation (capturing the spatial structure, as measured by Moran's I (Moran, 1950)). However, the SHI does not capture information about how the correlation varies with the distance between samples, and so the variogram is the preferred measure.

3. Results and discussion

3.1. Predictions of spatial remodelling patterns due to bronchoconstriction-mechanotransduction-remodelling (BMR) cycles

Fig. 3 illustrates the effects of BMR cycles in the model, showing the evolution of a typical flow pattern from a single simulation, as well as the emergence of a remodelling pattern after repeated cycles of bronchoconstriction, mechanotransduction, and remodelling. The top

row shows the evolution of remodelling (expressed here in terms of normalized wall area (WA)), evolving left to right; the lower row shows the same evolution steps in terms of flow. The bronchoconstriction which occurs in low flow regions leads to mechanotransduction and remodelling, and further remodelling of these airways makes them more prone to future bronchoconstriction in subsequent cycles. Fig. 4 shows the evolution of many such simulations over repeated cycles, in terms of a more simplified analysis, the spatial heterogeneity index (SHI) of normalized WA (left panel), the SHI of flow (center panel), and airway resistance (right panel). Recall that the SHI is an equally-weighted sum of the spatial autocorrelation and the coefficient of variation; it provides a simplified quantification of spatial heterogeneity but does not take into account the spatial scale of that heterogeneity. Clearly evolution of the remodelling process over repeated cycles significantly alters both the resistance and SHI of wall area, though no clear change is evident in the flow SHI, which begins with significant spatial heterogeneity. In comparison there is a rapid increase in SHI of WA from a relatively homogenous initial distribution. The contrast between Figs. 3 and 4 (centre panel) highlights the inadequacy of SHI as a measure of these patterns and supports the use of variograms to assess spatial correlations.

From Figs. 3 & 4 we see that the BMR cycles can alter the structure and function of the simulated lung. The exact character of these changes can be quantified more explicitly in terms of the variograms.

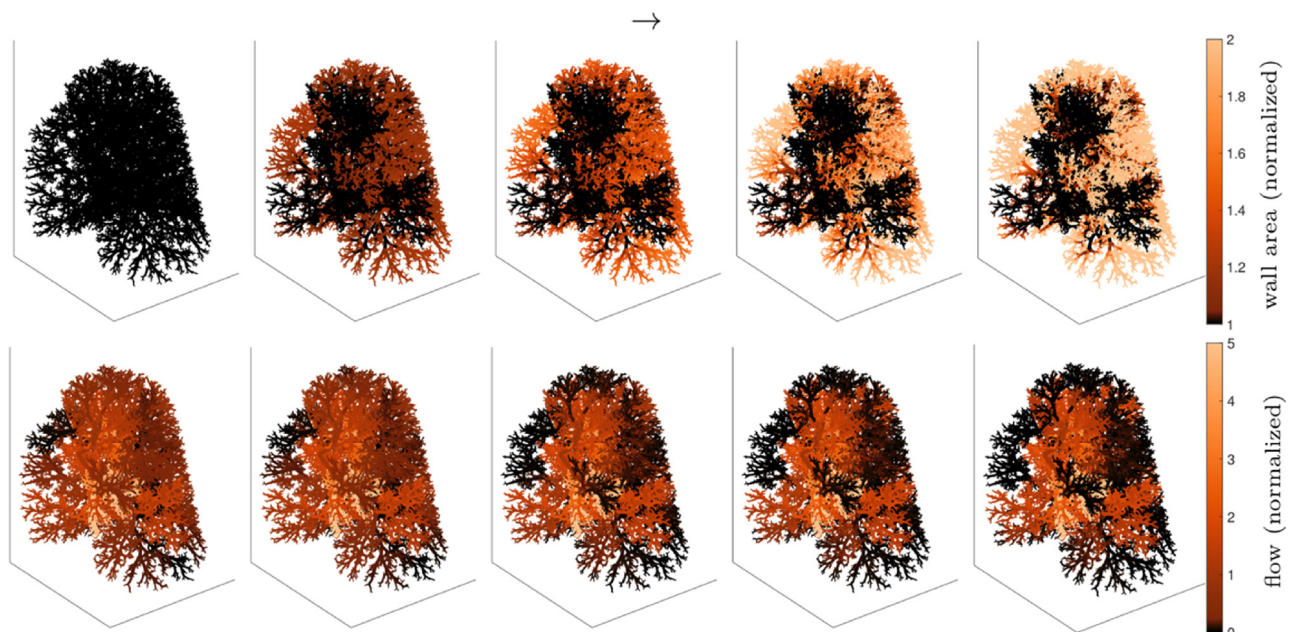


Fig. 3. Illustration of BMR cycles in a typical simulation; arrow indicates evolution over BMR cycles (left to right). Top row: WA spatial distribution, normalized to initial. Bottom row: corresponding flow patterns during bronchoconstriction phase, normalized to nominal (Donovan et al., 2018).

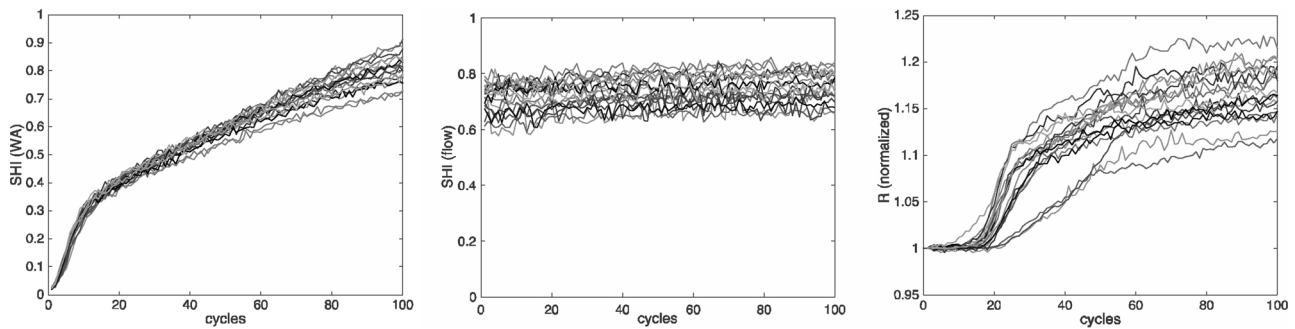


Fig. 4. Evolution of spatial heterogeneity in remodelling over 100 BMR cycles. Left: spatial heterogeneity index (SHI) based on wall area (WA); center: SHI based on flow; right: respiratory resistance (normalized). Each panel shows 25 independent simulations, starting from a structurally near-homogeneous initial state. Here $\delta = 0.025$.

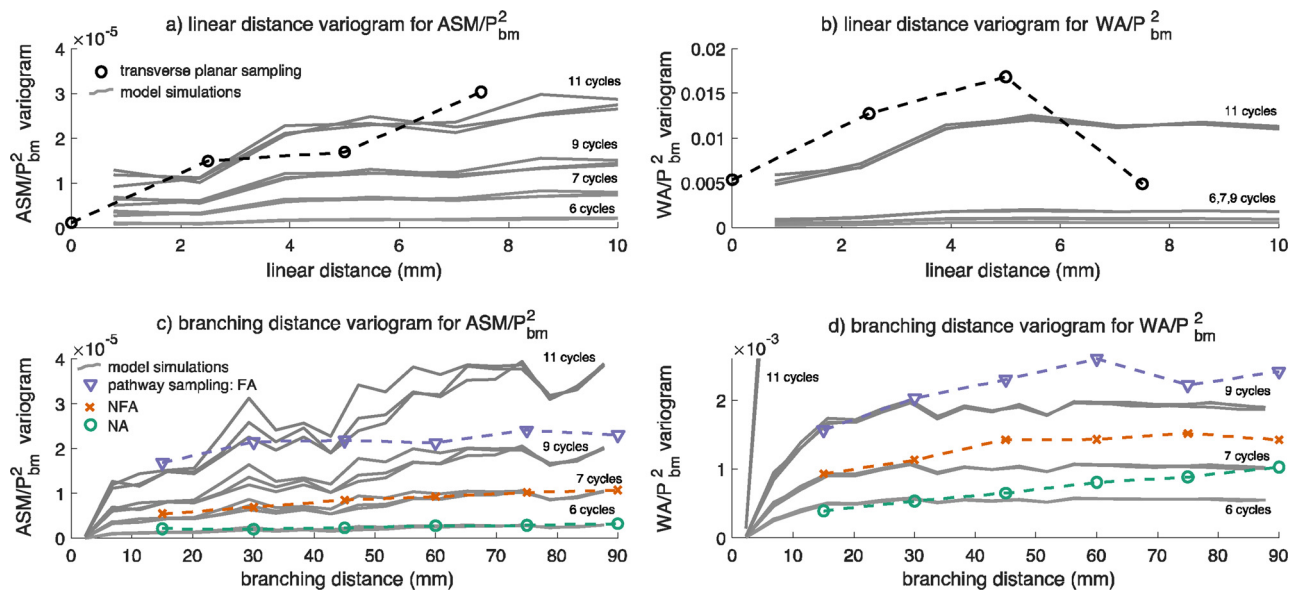


Fig. 5. Predicted BMR variograms (grey lines); left: ASM; right: WA. Upper: standard linear distance variogram. Lower: distance over branching airway tree variogram. Variograms from experimental data (dashed lines) overlaid for comparison. Transverse planar sampling data showing pairwise variation for normalized ASM depending on pair separation distance h , and variation for normalized WA; (a) corresponding ASM and (b) WA variogram; (c) and (d) branching distance variograms from pathway sampling data, classified as non-asthma (NA, green circles), non-fatal asthma (NFA, red x's) and fatal asthma (FA, blue triangles). Here variograms are shown after 6, 7, 9, and 11 BMR cycles, from 3 independent simulations. The groups are in monotonically increasing order.

Predicted remodelling variograms are given in Fig. 5. Two measures are expressed: the linear distance variogram (e.g. simple linear distance between airway pairs), and the branching distance variogram based on the distance between airways along the conducting airway tree (proximal end to proximal end). Here variograms are shown from 3 independent simulations (grey, solid lines) and after 6, 7, 9, and 11 BMR cycles. Recall that, as per the Methods, in whole-lung simulations we use a relatively large degree of remodelling per cycle, and hence a relatively small number of cycles. The important aspect is not the absolute number of cycles, but rather the progression with additional cycles. The results are qualitatively the same using a larger number of cycles and a smaller amount of remodelling per cycle, but this induces much greater computational cost. The most important aspect is that some number of BMR cycles can produce these spatial patterns. Intra-lobe airway pairs are classified by separation of anatomical levels, and the number of samples ranges from $n = 72$ (FA, maximum branching distance) to $n = 753$ (NFA, minimum branching distance). For purposes of comparison we have assumed a mean separation of 15 mm per anatomical level.

These predicted variograms can then be compared with the human airway data acquired via both pathway sampling and transverse planar sampling. Transverse planar sampling data is used to compute linear

distance variograms, up to the distance of reliability, and these are given in the black dashed lines in Fig. 5, panels a and b. Although these data are limited to short length scales ($\sim < 10$ mm separation), both WA and ASM data suggest a degree of spatial correlation in structure over this length scale. As outlined in Fig. 2, spatially-uncorrelated remodelling would yield a variogram which is constant with respect to the separation distance.

Transverse planar sampling sections (e.g. Fig. 1 left panel) contain airways such that the measured distance between airway pairs is the exact linear distance, allowing direct calculation of the linear distance variogram. Potential bias in airway selection is limited, with the only exclusion criterion being the angle at which the airway is “out of plane” with the slice. However, this methodology is limited to relatively short distances as airway pairs must be contained in the same 15–20 mm diameter core to be assessed. Sample size is also relatively low and is insufficient to differentiate between status and severity of asthma (asthma $n = 12$, non-asthma $n = 9$). Nonetheless, analysis of this data in terms of the variogram does suggest a dependent spatial relationship at scales up to ~ 10 mm.

To address limitations described above, longer length scales were assessed using intra-lobe airway pairs acquired through pathway sampling (e.g., Fig. 1 right panel). Variograms for both ASM and WA are

shown in Fig. 5 panels c and d. Because these data are sampled along the tree, the corresponding variograms are the branching distance variograms. Here the larger number of samples allows classification by group: non-asthma (NA, green circles), non-fatal asthma (NFA, red x's) and fatal asthma (FA, blue triangles). Here we have assumed a separation distance of 15 mm per anatomical level, for comparison. There is a clear distinction between the NA, NFA and FA populations expressed in this way, as well as an indication of the potential spatial pattern, in agreement with model predictions. That is, airways which are closer together (in terms of anatomical levels) appear to have greater correlation in ASM and WA, while those with greater separation have decreased correlation. An unbalanced two-way ANOVA analysis of the intra-lobe airway pairs (e.g. the experimental variograms in Fig. 5) indicates statistical significance for asthma status (NA, NFA, FA; $p < 0.0001$), branching distance ($p < 0.0001$) and interaction between asthma status and branching distance ($p = 0.02$).

Another way of interpreting this is to recall that the variogram captures how much the structure in two airways differ, averaged across all airway pairs which are a certain distance apart. If structure was uniform everywhere, then the variogram would be zero. Hence the magnitude of the variogram captures information about heterogeneity. Moreover it indicates how it is arranged spatially, in that airways which are near to one another are more similar (smaller variogram) while airways which are far from each other are less similar (larger variogram).

An alternative approach is to examine spatial associations using Pearson correlation coefficients between airway pairs separated by different distances (in terms of anatomical levels), and these data are given in Table 3. In all cases, airways separated by only one anatomical level have moderate to strong correlation (> 0.4), with correlations falling for airways separated by greater distances. For comparison, the Pearson coefficients for the model simulations are also shown, assuming a 15 mm branching distance per anatomical level. When comparing correlations derived from the model and experimental data, it is important to appreciate that greater numbers of model simulations are available compared with the experimental data, and that within the experimental data there are many more pairs separated by fewer anatomical levels.

It is thus clear that BMR cycles are a plausible explanation for the formation of the observed spatial correlations. Importantly, correlations are present in the NA population as well as the NFA and FA groups. This means that the underlying remodelling process must at least respect and maintain these spatial correlations, if not increase them; if a remodelling processes occurred which was completely independent of these initial spatial correlations, the variograms would be expected to become independent of the separation distance (e.g. have slope zero).

An alternate approach to this analysis is to normalise WA/Pbm^2 and ASM/Pbm^2 to the averages for each subject. Repeating the above analysis using this approach does not alter the results. An extensive sensitivity analysis of the model was performed with respect to parameters

Table 3

Pearson correlation coefficients for WA/Pbm^2 between airway pairs separated by h anatomical levels. Model results are the same to two significant figures for 6,7,8 and 11 cycles (those shown in Fig. 5.). For purposes of comparison, a 15 mm branching distance per anatomical level is assumed.

	h = 1 level	2	3	4	5	6	7	h = 8 levels
NA	0.51 [§]	0.31 [§]	0.17 [#]	0.06	0.03	0.05	0.08	0.28*
NFA	0.41 [§]	0.28 [§]	0.17 [§]	0.17 [#]	0.05	0.08	0.002	0.008
FA	0.36 [§]	0.16 [#]	0.002	-0.07	-0.05	-0.06	0.01	0.10
Model	0.41 [§]	0.38 [§]	0.38 [§]	0.37 [§]	0.36 [§]	0.36 [§]	0.38 [§]	0.38 [§]

* = $p < 0.01$.

= $p < 0.001$.

§ = $p < 0.0001$.

for degree of ASM activation during challenge, degree of airway-parenchymal interdependence, rate of bronchoconstriction-induced remodelling, and strength of additive white noise per cycle (see methods). In all cases the results remain qualitatively consistent with the results for the parameter set shown.

It is important to appreciate that pathway sampling of the airways introduces the variable of airway size, or Pbm (basement membrane length) as is conventionally used in histological studies on airway tissue. The axial airways (i.e. longest path) at anatomical levels 6–9 are comprised of large central airways, (defined as having cartilage and mucous glands in their walls), whilst those at anatomical levels 1–3 are classified as small airways, and lack these features. Airways in the intermediate zone (levels 4–6) exhibit transitional features. Given the very large number of samples in this analysis it was possible to extract useful information from the computed variograms. Here it is striking to notice not only the pattern of increasing variation with separation distance, but also the clear distinction between NA, NFA and FA groups.

While variograms generated from transverse planar or pathway sampling have different limitations (and strengths), a clear picture is emerging: it seems probable that spatial correlations in airway remodelling exist, and that the specific spatial correlation patterns are consistent with those which might be expected if the underlying process of formation is repeated BMR cycles. Other mechanisms, including those derived from inflammatory signals, could also be consistent, if there are local mechanisms to drive such spatial correlations.

Eosinophil and neutrophil counts were available for a subset of the pathway sampling data ($N = 217$ airways). Analysis of this subset of data suggested similar spatial correlations for inflammatory cells. Although the relative size of this data subset makes more extensive analysis impossible, these cell count data suggest that inflammatory processes are also spatially correlated, particularly in more severe asthma. Eosinophil and neutrophil count, normalised to wall area, were not significantly correlated with WA/Pbm^2 ($\rho = 0.12$, $p = 0.08$), but ASM/Pbm^2 showed a modest correlation which did reach significance ($\rho = 0.23$, $p < 0.05$).

3.2. Clinical implications and testing these hypotheses in patients

The above analyses provide evidence to support correlations in airway remodelling and also predicts the specific statistical signature that would be expected if airway remodelling was driven by a BMR-type process. That is, remodelling produced by functional behaviour such as bronchoconstriction to an environmental trigger, when repeated over many cycles, will yield a variogram dependent on separation distance. In comparison, remodelling that occurs through a mechanism which does not lead to spatial correlations in airway structure – for example, if remodelling simply occurred at (independent) random sites – would exhibit variograms without any dependence on the separation distance.

Present findings have potential implications for the treatment of remodelling in asthma. If remodelling is to be considered a therapeutic target, understanding the mechanism of formation provides an opportunity to reverse, or – perhaps of greater significance – prevent disease. Actively targeting the remodelling process at an early stage might be most effective in reducing the consequences of remodelling, and this could have implications for selection of short- or long-acting therapies. However, there is mounting evidence that airway remodelling is acquired very early in life and lung function is impaired at birth in subjects who go on to develop asthma (Håland et al., 2006), indicating that the BMR cycles and the resulting spatially correlated remodelling may occur *in utero*. If airway remodelling developed in this manner, successful intervention would be more difficult and require prenatal application.

Spatially correlated airway remodelling provides explanation for various functional abnormalities that have been documented in patients with asthma. Lung ventilation defects are detected by hyperpolarized

³He MRI in asthmatic patients which persist over time (de Lange et al., 2007, 2009) which is consistent with regions of clustered airway remodelling. Spatially correlated remodelling is also important to understand for therapies like bronchial thermoplasty (Cox et al., 2007; Pavord et al., 2007; Castro et al., 2010; Donovan et al., 2018) in which specific airways are targeted. That is, treating regions of the lung that actually exhibits airway remodelling is of interest to the patient.

Obtaining more comprehensive data from subjects with asthma would allow for assessment of relevant statistical signatures in patients from different ages. This would allow for investigation into the age at which these spatial correlations develop. In vivo this might be achieved through CT (Castro et al., 2011) or optical coherence tomography (OCT) (de Lange et al., 2007, 2009; Li et al., 2018) for wall area, with polarization-sensitive OCT (PS-OCT) (Adams et al., 2016) providing an option for differentiating ASM. Ex vivo measurement would also be possible with appropriate sampling and distance measurements.

3.3. Limitations and future directions

The effect of airway size on study conclusions requires more explicit discussion. Certainly other work has suggested the potential importance of differential remodelling in large vs small airways (Hirota and Martin, 2013; Elliot et al., 2015), and such an outcome would be intrinsically linked with spatial correlations due to their relationships in the structure of the airway tree. We have treated airways of different size equally by normalizing both ASM and WA by the square of Pbm, such that the quantities are dimensionless. Differential responses in airways of different size (e.g. that do not scale in this dimensionless way) would further complicate the analysis of correlated remodelling but would also enable potentially interesting phenomena such as propagation of large airway remodelling toward more distal airways (James et al., 2012; Elliot et al., 2015). It is also worth noting the difference in age between the pathway sampling and transverse planar sampling groups; the latter tended to be younger, potentially introducing effects associated with maturation or childhood phenotypes of asthma.

Another assumption in the model that bears further discussion relates to baseline airway structure in subjects with and without asthma i.e., before BMR cycles are imposed. There was no distinction between subjects with or without asthma in the conceptual model, in that all simulated BMR remodelling patterns emerged from a homogeneous background state via a self-organized process (Venegas et al., 2005) and differ only by the number of BMR cycles. However, it is clear from Fig. 5 that spatially correlated remodelling patterns associated with different states might emerge from the same underlying process with slightly different details, for example that NA, NFA and FA lung structures might only be separated by the number and/or severity of BMR cycles. That is, even NA lungs appear to have spatial correlations, but these must be respected and reinforced by the remodelling processes which result in progression to NFA and FA. If the remodelling processes were entirely independent of the spatial relationships, the spatial correlations apparent even in NA would be expected to fall with disease progression. Additionally, early life events (*in utero*), which predispose individuals to developing asthma, may alter the development of the lung such that people with asthma start at a different baseline from those without asthma making them more susceptible to the effects of BMR cycles. Again, this could manifest as spatially correlated airway remodelling which is present in the first year of life as opposed to developing throughout childhood and adolescence.

One limitation in the model is that the actual amount of remodelling per cycle is largely unknown. This is strongly mitigated by the fact that equivalent results are obtained using either a small number of cycles with a large degree of remodelling per cycle, or a larger number of cycles with a smaller amount of remodelling per cycle. It does, however, mean that the specific number of BMR cycles indicated is irrelevant; what is important is the progression with additional cycles. Similarly, the balance between WA remodelling and ASM remodelling

is largely unknown. We have also assumed that BMR cycles are always either neutral or detrimental to airway structure – that is, every airway either stays the same, or gets worse, as the result of a BMR cycle. If remodelling is instead a reversible or self-limiting process, as is perhaps likely in some form, the consequences of this process could differ considerably. A reversible aspect of the remodelling process would likely allow equilibration of the remodelling pattern, meaning that the spatial correlation pattern would stabilize after some number of cycles, although the statistical signature would be expected to remain qualitatively similar to those considered in this study.

Assessment of inflammatory correlations is another interesting avenue of investigation. A comprehensive dataset on inflammation was not available from these patients, although we analysed preliminary data from a subset of 217 airways. Early findings report similar spatial correlations in inflammation (eosinophil and neutrophils) which should be confirmed in a larger, more focused study.

4. Conclusions

Taken together, these results suggest that airway remodelling in asthma may have significant spatial correlations, and that one plausible origin of these spatial correlations is via an underlying mechanism consisting of cycles of bronchoconstriction, mechanotransduction, and remodelling. Other underlying mechanisms, such as inflammatory pathways, are possible, but the spatial correlations seen in all disease states suggest that *any* plausible underlying processes, whether BMR or inflammatory, *in utero* or later in life, must respect and maintain these spatial correlations: a spatially-independent remodelling process would lead to *decreases* in the apparent spatial correlations with disease progression. Moreover, spatial correlations in airway remodelling are expected to have a significant impact on resulting lung function. Identifying and understanding the evolution of spatial correlations in airway remodelling in asthma should be considered and may be relevant when developing strategies to mitigate disease severity.

Author contributions

GMD constructed the model, performed simulations, analysed the data and was responsible for overall design. CDP, FHYG, JGE and ALJ acquired the experimental data. CDP, PBN, and GMD drafted the manuscript. All authors reviewed the manuscript.

Data availability

The datasets generated during and/or analysed during the current study are available from the corresponding author on reasonable request.

Declaration of Competing Interest

The authors declare no competing interests.

Acknowledgements

GMD acknowledges support from the Royal Society of New Zealand via the Marsden Fund. PBN was supported by a Western Australian Department of Health - Merit Award and a Medical and Health Research Infrastructure Fund.

Appendix A. additional morphometry details

The collection of the transverse planar sampling data has previously been described (Chin et al., 2012). Briefly, a grid of approximately 3500 points was overlaid on digitized images of the airways and points that fell on the area of interest were counted. There were approximately 2.3

points per 1000 μm^2 , and the density of the point grid was internally validated as previously described (ref (Chin et al., 2012) *supplementary material*). Multiplying the ratio of points that fall on the region of interest by the size of the image (in mm^2) yielded the area for that layer. The final area values (ASM and total wall area, (WA) were normalized to Pbm^2 to control for differences in airway size. Pbm was determined by manually tracing the perimeter (ImageScope, Leica Biosystems).

Morphometry of airways acquired by pathway sampling was conducted on sections stained with the elastic trichrome technique. Point counting was performed using a Nikon light microscope, drawing tube and square lattice grid containing 240 points. The point counts for each feature were converted to area fractions using the formula: Area (mm^2) = Z^2x (point count value) where Z^2 was a constant derived from the distance between two points on the grid x a magnification factor. The perimeter of the airway was determined from the number of intersections between the grid lines and the luminal aspect of the basement membrane. The intersection counts were converted to a length (perimeter) mm using the formula: Perimeter = $Z \times$ number of intersections (Howard and Reed, 2004).

References

- Adams, D.C., Hariri, L.P., Miller, A.J., Wang, Y., Cho, J.L., Villiger, M., Holz, J.A., Szabari, M.V., Hamilos, D.L., Scott Harris, R., Griffith, J.W., Bouma, B.E., Luster, A.D., Medoff, B.D., Suter, M.J., 2016. Birefringence microscopy platform for assessing airway smooth muscle structure and function in vivo. *Sci. Transl. Med.* 8 359ra131.
- Anafi, R.C., Wilson, T.A., 2001. Airway stability and heterogeneity in the constricted lung. *J. Appl. Physiol.* 91, 1185–1192.
- Bai, T.R., Roberts, C.R., Paré, P.D., 1998. Airway remodelling. *Asthma*. pp. 475–486.
- Boser, S.R., Park, H., Perry, S.F., Ménache, M.G., Green, F.H.Y., 2005. Fractal geometry of airway remodeling in human asthma. *Am. J. Respir. Crit. Care Med.* 172, 817–823.
- Castro, M., Rubin, A.S., Laviolette, M., Fiterman, J., De Andrade Lima, M., Shah, P.L., Fiss, E., Olivenstein, R., Thomson, N.C., Niven, R.M., Pavord, I.D., Simoff, M., Duhamel, D.R., McEvoy, C., Barbers, R., Ten Hacken, N.H.T., Wechsler, M.E., Holmes, M., Phillips, M.J., Erzurum, S., Lunn, W., Israel, E., Jarjour, N., Kraff, M., Shargill, N.S., Quiring, J.J., Berry, S.M., Cox, G., AIR2 Trial Study Group, 2010. Effectiveness and safety of bronchial thermoplasty in the treatment of severe asthma: a multicenter, randomized, double-blind, sham-controlled clinical trial. *Am. J. Respir. Crit. Care Med.* 181, 116–124.
- Castro, M., Fain, S.B., Hoffman, E.A., Gierada, D.S., Erzurum, S.C., Wenzel, S., 2011. National Heart, Lung, and Blood Institute's Severe Asthma Research Program, 2011. Lung imaging in asthmatic patients: the picture is clearer. *J. Allergy Clin. Immunol.* 128, 467–478.
- Chin, L.Y.M., Bossé, Y., Pascoe, C., Hackett, T.L., Seow, C.Y., Paré, P.D., 2012. Mechanical properties of asthmatic airway smooth muscle. *Eur. Respir. J.* 40, 45–54.
- Cox, G., Thomson, N.C., Rubin, A.S., Niven, R.M., Corris, P.A., Siersted, H.C., Olivenstein, R., Pavord, I.D., McCormack, D., Chaudhuri, R., Miller, J.D., Laviolette, M., AIR Trial Study Group, 2007. Asthma control during the year after bronchial thermoplasty. *N. Engl. J. Med.* 356, 1327–1337.
- Cressie, N., Hawkins, D.M., 1980. Robust estimation of the variogram: I. *J. Int. Assoc. Math. Geol.* 12, 115–125.
- de Lange, E.E., Altes, T.A., Patrie, J.T., Parmar, J., Brookeman, J.R., Mugler 3rd, J.P., Platts-Mills, T.A.E., 2007. The variability of regional airflow obstruction within the lungs of patients with asthma: assessment with hyperpolarized helium-3 magnetic resonance imaging. *J. Allergy Clin. Immunol.* 119, 1072–1078.
- de Lange, E.E., Altes, T.A., Patrie, J.T., Battiston, J.J., Juersivich, A.P., Mugler 3rd, J.P., Platts-Mills, T.A., 2009. Changes in regional airflow obstruction over time in the lungs of patients with asthma: evaluation with ^3He MR imaging. *Radiology* 250, 567–575.
- Donovan, G.M., 2016. Clustered ventilation defects and bilinear respiratory reactivity in asthma. *J. Theor. Biol.* 406, 166–175.
- Donovan, G.M., 2017. Inter-airway structural heterogeneity interacts with dynamic heterogeneity to determine lung function and flow patterns in both asthmatic and control simulated lungs. *J. Theor. Biol.* 435, 98–105.
- Donovan, G.M., Kritter, T., 2015. Spatial pattern formation in the lung. *J. Math. Biol.* 70, 1119–1149.
- Donovan, G.M., Elliot, J.G., Green, F.H.Y., James, A.L., Noble, P.B., 2018. Unravelling a clinical paradox - why does bronchial thermoplasty work in asthma? *Am. J. Respir. Cell Mol. Biol.* <https://doi.org/10.1165/rncmb.2018-00110C>.
- Elliot, J.G., Jones, R.L., Abramson, M.J., Green, F.H., Mauad, T., McKay, K.O., Bai, T.R., James, A.L., 2015. Distribution of airway smooth muscle remodelling in asthma: relation to airway inflammation. *Respirology* 20, 66–72.
- Fabry, B., Fredberg, J.J., 2007. Mechanotransduction, asthma, and airway smooth muscle. *Drug Discov. Today Dis. Models* 4, 131–137.
- Gillis, H.L., Lutchen, K.R., 1999. How heterogeneous bronchoconstriction affects ventilation distribution in human lungs: a morphometric model. *Ann. Biomed. Eng.* 27, 14–22.
- Grainge, C.L., Lau, L.C.K., Ward, J.A., Dulay, V., Lahiff, G., Wilson, S., Holgate, S., Davies, D.E., Howarth, P.H., 2011. Effect of bronchoconstriction on airway remodeling in asthma. *N. Engl. J. Med.* 364, 2006–2015.
- Green, F.H.Y., Williams, D.J., James, A., McPhee, L.J., Mitchell, I., Mauad, T., 2010. Increased myoepithelial cells of bronchial submucosal glands in fatal asthma. *Thorax* 65, 32–38.
- Håland, G., Carlsen, K.C.L., Sandvik, L., Devulapalli, C.S., Munthe-Kaas, M.C., Pettersen, M., Carlsen, K.-H., Oraacle, 2006. Reduced lung function at birth and the risk of asthma at 10 years of age. *N. Engl. J. Med.* 355, 1682–1689.
- Hessel, P.A., Mitchell, I., Tough, S., Green, F.H.Y., Cockcroft, D., Kepron, W., Butt, J.C., 1999. Risk factors for death from asthma. *Ann. Allergy Asthma Immunol.* 83, 362–368.
- Hill, M.R., Philp, C.J., Billington, C.K., Tatler, A.L., Johnson, S.R., O'Dea, R.D., Brook, B.S., 2018. A theoretical model of inflammation- and mechanotransduction-driven asthmatic airway remodelling. *Biomech. Model. Mechanobiol.*
- Hirota, N., Martin, J.G., 2013. Mechanisms of airway remodeling. *Chest* 144, 1026–1032.
- Howard, V., Reed, M., 2004. Unbiased stereology: three-dimensional measurement in microscopy. Garland Science.
- Howatson Tawhai, M., Pullan, A.J., Hunter, P.J., 2000. Generation of an anatomically based three-dimensional model of the conducting airways. *Ann. Biomed. Eng.* 28, 793–802.
- James, A.L., Wenzel, S., 2007. Clinical relevance of airway remodelling in airway diseases. *Eur. Respir. J.* 30, 134–155.
- James, A.L., Paré, P.D., Hogg, J.C., 1988. Effects of lung volume, bronchoconstriction, and cigarette smoke on morphometric airway dimensions. *J. Appl. Physiol.* 64, 913–919.
- James, A.L., Green, F.H., Abramson, M.J., Bai, T.R., Dolnikoff, M., Mauad, T., McKay, K.O., Elliot, J.G., 2008. Airway basement membrane perimeter distensibility and airway smooth muscle area in asthma. *J. Appl. Physiol.* 104, 1703–1708.
- James, A.L., Elliot, J.G., Jones, R.L., Carroll, M.L., Mauad, T., Bai, T.R., Abramson, M.J., McKay, K.O., Green, F.H., 2012. Airway smooth muscle hypertrophy and hyperplasia in asthma. *Am. J. Respir. Crit. Care Med.* 185, 1058–1064.
- Kılıç, A., Ameli, A., Park, J.A., Kho, A.T., Tantisira, K., Santolini, M., Cheng, F., Mitchell, J.A., McGill, M., O'Sullivan, M.J., De Marzio, M., et al., 2020. Mechanical forces induce an asthma gene signature in healthy airway epithelial cells. *Sci. Rep.* 10 (1), 1–12.
- Lai-Fook, S.J., 1977. Lung parenchyma described as a prestressed compressible material. *J. Biomech.* 10, 357–365.
- Lambert, R.K., Wilson, T.A., Hyatt, R.E., Rodarte, J.R., 1982. A computational model for expiratory flow. *J. Appl. Physiol.* 52, 44–56.
- Leary, D., Winkler, T., Braune, A., Maksym, G.N., 2014. Effects of airway tree asymmetry on the emergence and spatial persistence of ventilation defects. *J. Appl. Physiol.* 117, 353–362.
- Li, Q., Karnowski, K., Noble, P.B., Cairncross, A., James, A., Villiger, M., Sampson, D.D., 2018. Robust reconstruction of local optic axis orientation with fiber-based polarization-sensitive optical coherence tomography. *Biomed. Opt. Express* 9, 5437–5455.
- Lutchen, K.R., 2016. Invited Editorial on "Measurement of intraindividual airway tone heterogeneity and its importance in asthma": how does an airway and subsequently the lung become hyperresponsive? *J. Appl. Physiol.* 121, 221–222.
- Lutchen, K.R., Paré, P.D., Seow, C.Y., 2017. Hyperresponsiveness: relating the intact airway to the whole lung. *Physiology* 32, 322–331.
- Moran, P.A.P., 1950. Notes on continuous stochastic phenomena. *Biometrika* 37, 17–23.
- Omre, H., 1984. The variogram and its estimation. *Geostatistics for Natural Resources Characterization*. pp. 107–125.
- Parvez, O., Voss, A.M., De Kok, M., Roth-Kleiner, M., Belik, J., 2006. Bronchial muscle peristaltic activity in the fetal rat. *Pediatr. Res.* 59 (6), 756–761.
- Pascoe, C.D., Obeidat, M., en, Arsenault, B.A., Nie, Y., Warner, S., Stefanowicz, D., Wadsworth, S.J., Hirota, J.A., Jasmine Yang, S., Dorscheid, D.R., Carlsten, C., Hackett, T.L., Seow, C.Y., Paré, P.D., 2017a. Gene expression analysis in asthma using a targeted multiplex array. *BMC Pulm. Med.* 17, 189.
- Pascoe, C.D., Seow, C.Y., Hackett, T.L., Paré, P.D., Donovan, G.M., 2017b. Heterogeneity of airway wall dimensions in humans: a critical determinant of lung function in asthmatics and nonasthmatics. *Am. J. Physiol. Lung Cell Mol. Physiol.* 312, L425–L431.
- Pavord, I.D., Cox, G., Thomson, N.C., Rubin, A.S., Corris, P.A., Niven, R.M., Chung, K.F., Laviolette, M., RISA Trial Study Group, 2007. Safety and efficacy of bronchial thermoplasty in symptomatic, severe asthma. *Am. J. Respir. Crit. Care Med.* 176, 1185–1191.
- Redington, A.E., Howarth, P.H., 1997. Airway wall remodelling in asthma. *Thorax* 52, 310–312.
- Salkie, M.L., Mitchell, I., Revers, C.W., Karkhanis, A., Butt, J., Tough, S., Green, F.H., 1998. Postmortem serum levels of trypsinase and total and specific IgE in fatal asthma. *Allergy Asthma Proc.* 19, 131–133.
- Stewart, A.G., 1996. Airway Wall Remodelling in Asthma. CRC Press.
- Syyong, H.T., Pascoe, C.D., Zhang, J., Arsenault, B.A., Solomon, D., Elliott, W.M., Hackett, T.L., Walker, D.C., Paré, P.D., Seow, C.Y., 2015. Ultrastructure of human tracheal smooth muscle from subjects with asthma and nonasthmatic subjects. Standardized methods for comparison. *Am. J. Respir. Cell Mol. Biol.* 52, 304–314.
- Tgavalekos, N.T., Tawhai, M., Harris, R.S., Musch, G., Mush, G., Vidal-Melo, M., Venegas, J.G., Lutchen, K.R., 2005. Identifying airways responsible for heterogeneous ventilation and mechanical dysfunction in asthma: an image functional modeling approach. *J. Appl. Physiol.* 99, 2388–2397.
- Thorpe, C.W., Bates, J.H., 1997. Effect of stochastic heterogeneity on lung impedance during acute bronchoconstriction: a model analysis. *J. Appl. Physiol.* 82, 1616–1625.
- Tough, S.C., Green, F.H.Y., Paul, J.E., Wigle, D.T., Butt, J.C., 1996. Sudden death from asthma in 108 children and young adults. *J. Asthma Allergy* 33, 179–188.
- Tschumperlin, D.J., Drazen, J.M., 2006. Chronic effects of mechanical force on airways. *Annu. Rev. Physiol.* 68, 563–583.
- Venegas, J.G., Winkler, T., Musch, G., Vidal Melo, M.F., Layfield, D., Tgavalekos, N., Fischman, A.J., Callahan, R.J., Bellani, G., Harris, R.S., 2005. Self-organized patchiness in asthma as a prelude to catastrophic shifts. *Nature* 434, 777–782.